Anisotropy of electrical conductivity record of initial strain at the toe of the Nankai accretionary wedge

Pierre Henry, Laurence Jouniaux, Elizabeth Screaton, Sabine Hunze, Demian Saffer

Anisotropy of electrical conductivity record of initial strain at the toe of the Nankai accretionary wedge

Pierre Henry[1,2] Laurence Jouniaux,[1] Elizabeth J. Screaton,[3] Sabine Hunze,[4] and Demian M. Saffer[5]

Received 4 November 2002; revised 1 April 2003; accepted 9 May 2003; published 3 September 2003.

[1] An approach based on March's theory is applied to measurements of the anisotropy of electrical conductivity on samples and is used to quantify initial strain at the toe of the Nankai accretionary wedge. A quantitative determination of strain is possible from simple assumptions: passive reorientation of flat pores forming the porous network and existence of a linear relationship between fabric tensor and electrical conductivity tensor. We show that this simple model correctly accounts for the increase of anisotropy with compaction at a reference site located in the trench (Ocean Drilling Program drill Site 1173). At the toe of the accretionary wedge (Site 1174), development of anisotropy in the horizontal plane and concurrent reduction of vertical plane anisotropy are observed. This can be explained by 12% horizontal ductile shortening, occurring after decollement initiation but before slip on imbricate thrust faults. Anisotropy in the underthrust sequence is correctly described by vertical compaction, consistent with decoupled stress states across the decollement. At Site 1174 the magnitude of ductile strain implies at least 75 m slip on the decollement. Ductile shortening is associated with porosity loss, implying partly drained conditions above the decollement. *INDEX TERMS:* 8105 Tectonophysics: Continental margins and sedimentary basins (1212); 3022 Marine Geology and Geophysics: Marine sediments—processes and transport; 8094 Structural Geology: Instruments and techniques; 5109 Physical Properties of Rocks: Magnetic and electrical properties; *KEYWORDS:* anisotropy of electrical conductivity, decollement, Nankai, strain, accretionary wedge

Citation: Henry, P., L. Jouniaux, E. J. Screaton, S. Hunze, and D. M. Saffer, Anisotropy of electrical conductivity record of initial strain at the toe of the Nankai accretionary wedge, *J. Geophys. Res.*, *108*(B9), 2407, doi:10.1029/2002JB002287, 2003.

1. Introduction

[2] Mechanical decoupling is essential for subduction and mountain building processes. Understanding how a synsedimentary or crustal decollement forms is thus an important problem in tectonics and geodynamics. One question asked is where decollement initiation occurs and how far ahead of the thrust front. In one extreme case, the decollement is a preexisting surface of mechanical decoupling and this discontinuity controls the deformation pattern from the beginning [e.g., *Beaumont and Quinlan*, 1994; *Doin and Henry*, 2001; *Karig and Morgan*, 1994]. Imbricate thrusting above a decollement may then be understood as a strain localization process of the bifurcation type [*Besuelle*, 2001; *Rudnicki and Rice*, 1975]. Alternatively, accretion of a new tectonic unit could be considered as one event, comprising stepwise decollement propagation, folding and thrusting. For example, accretion of new units could occur by fault propagation folding [*Allmendinger*, 1998; *Suppe*, 1985]. Processes may be distinguished from the pattern of early ductile strain. If mechanical decoupling occurs early, subhorizontal ductile shortening (also called layer parallel shortening) should occur within the section above the decollement before strain localization on thrust faults [*Averbuch et al.*, 1992; *Frizon de Lamotte*, 2002; *Sagnotti et al.*, 1998]. In fault propagation folding, ductile strain is associated with the folding and should concentrate in the forelimb of the folds [*Saint-Bezar et al.*, 2001]. Accretionary wedge toes are a special case of active fold and thrust belts, occurring under water and composed of high porosity sediments (30–70%). Because of this high water content and of their mechanical weakness, these sediments have the potential to record large ductile strains. They thus present an ideal case to study decollement initiation and imbricate thrusting. Studies of accretionary wedge toes by drilling have shown that ductile horizontal strain occurs in the toe region or in the trench and suggest early mechanical decoupling at the decollement level [*Housen*, 1997; *Morgan and Karig*, 1995a, 1995b; *Owens*, 1993]. Quan-

[1]Laboratoire de Géologie de l'Ecole Normale Supérieure, CNRS UMR 8538, Paris, France.
[2]Now at Departement de Geodynamique, College de France, Aix en Provence, France.
[3]Department of Geology, University of Florida, Gainesville, Florida, USA.
[4]Geowissenschaftliche Gemeinschaftsaufgaben-GCA, Hannover, Germany.
[5]Department of Geology and Geophysics, University of Wyoming, Laramie, Wyoming, USA.

0148-0227/03/2002JB002287$09.00

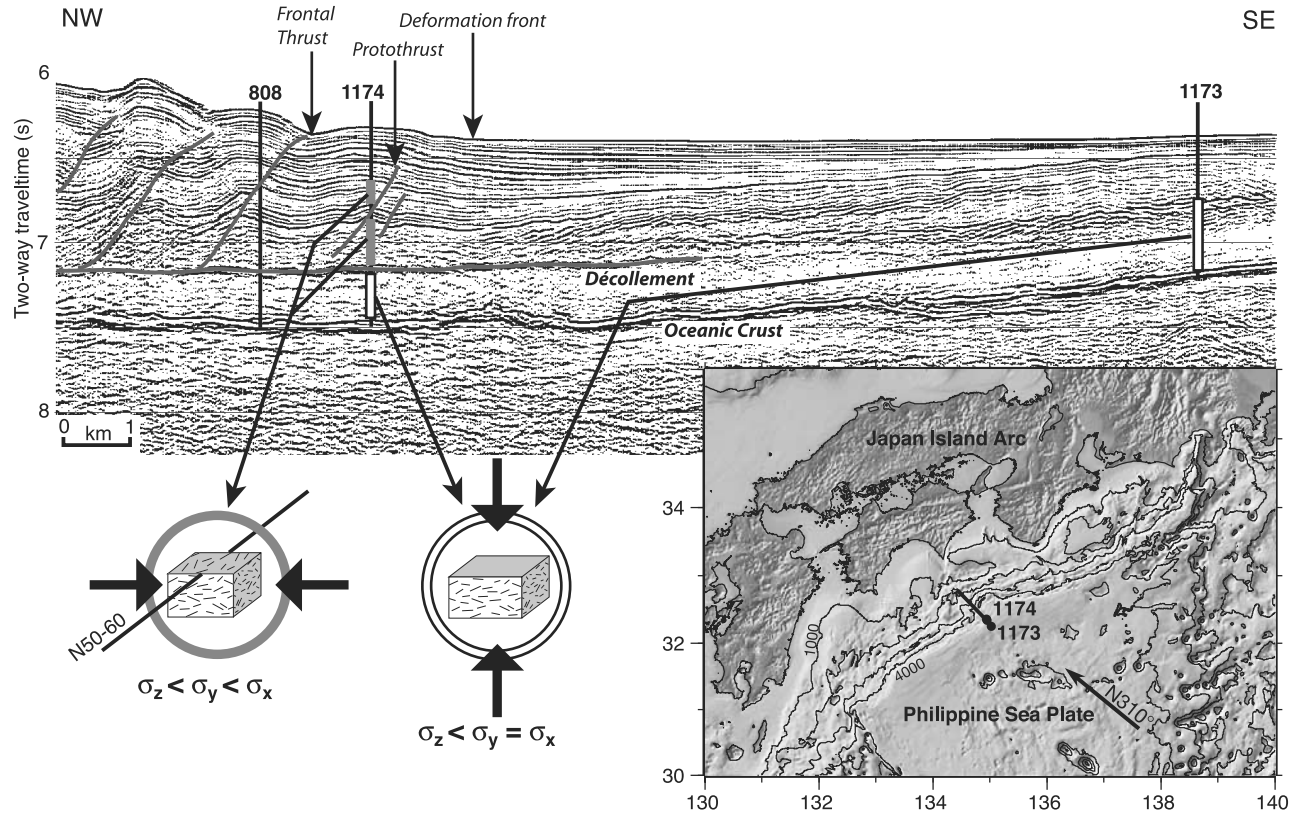

Figure 1. Location map and cross section of the toe of Nankai accretionary complex with the location of drill sites. Arrow on map shows N310° direction of Philippine Sea plate subduction. Results of anisotropy of electrical conductivity study are summarized. Vertical compaction occurs at Site 1173 and below the decollement level at Site 1174 (white bars). Sediments above the decollement (gray bars) record an additional component of horizontal strain.

tification of strain and determination of strain distribution and timing remain important problems.

[3] The anisotropy of magnetic susceptibility (AMS) is a commonly used indicator of strain [*Owens and Bamford*, 1976]. This measurement is very sensitive and has the advantage of yielding a complete six-component tensor. However, it is not, in general, used as a quantitative measurement of strain, in part because the mechanisms by which sediments acquire AMS are complex [*Rochette et al.*, 1992]. AMS as well as several other methods of strain determination have been tried at Site 808 at the toe of Nankai wedge, with ambiguous results [*Owens*, 1993; *Morgan and Karig*, 1993; *Brueckmann et al.*, 1993]. X-ray diffraction goniometry is a classic method of strain determination in sediment samples rich in layered silicates [*Evans et al.*, 1989]. This method indicates about 10% ductile horizontal shortening over the entire wedge section at Ocean Drilling Program (ODP) Site 808, but failed to give the correct vertical compaction strain component [*Morgan and Karig*, 1993]. Analyses of seismic profiles suggest a higher horizontal shortening in the trench, of 15–30% [*Morgan and Karig*, 1995a]. However, this latter value probably includes the effect of small-scale strain localization structures (faults or deformation bands), which are below seismic resolution. It should thus be considered as an upper bound to ductile strain. Anisotropy of *P* wave velocity has been measured on sample cubes during Leg 131 and appears to be affected by tectonic strain [*Brueckmann et al.*, 1993]. However, *P* wave anisotropy in the horizontal plane is too weak and noisy to be used for strain quantification. Electrical conductivity anisotropy is about 10 times larger and thus is easier to measure. Experimental work shows the anisotropy of electrical conductivity in clays follows strain, at least qualitatively [*Kuganenthira et al.*, 1996]. However, this property has been rarely used to assess strain in natural sediments.

[4] We here extend March's theory to include anisotropy of electrical conductivity measurements as the parameter measured to infer strain. In this approach, both clay particles and pores are idealized as flat disks, and reorganization with strain is treated as a passive rotation of the disks. This method is tested against data from the toe of Nankai accretionary wedge and yields consistent vertical and horizontal strain estimates. The deformation front of the wedge is defined by the onset of brittle deformation features (i.e., small scale faults) within the section above the decollement. The deformation front does not coincide with the frontal thrust, which is defined at the outcrop of the first thrust connecting the decollement and the seafloor (Figure 1). Site 808 was drilled through the frontal thrust during ODP Leg 131. Site 1174 was drilled during ODP Leg 190 in the zone between the deformation front and the frontal thrust, 1.8 km trenchward of Site 808 and

about 1.5 km landward of the deformation front. Site 1174 is thus a better location to study the onset of brittle deformation within the wedge section. At this location, two thrusts apparently offset sedimentary reflectors, and structural observations on cores define a zone of folding and fracturing between 463 and 500 meters below the seafloor (mbsf) that is designated as the protothrust [*Moore et al.*, 2001]. Site 1173 is a reference site located in the abyssal plain 14 km seaward of Site 808 and no compressive tectonic deformation is expected there. The present study is based on electrical conductivity measurements obtained at Sites 1173 and 1174. No anisotropy of electrical conductivity data are available at Site 808, which was drilled during an earlier cruise. However, electrical conductivity results from Site 1174 and Site 1173 alone are conclusive, and are compared with independent AMS and X-ray goniometry results.

2. Measurements

2.1. Method

[5] Complex electrical impedance of cubic samples cut from the core was measured on board the drill ship (Joides Resolution) with an impedance meter (Wayne-Kerr component analyzer), using two stainless steel electrodes [*Henry*, 1997; *Moore et al.*, 2001]. Filter papers soaked in seawater assured electrical contact between electrodes and sample. A zero reading was taken each time by measuring the impedance of the stacked two filters after they have been in contact with the sample. A frequency range of 20–30 kHz was selected for the measurements to minimize the imaginary part of the impedance, resulting in a phase angle of less than 3°. Conductivity along a given direction is computed from the real part of the conductance measured along this direction and from the dimensions of the sample. The three dimensions of the sample were measured with a caliper and are precise to within 0.1 mm.

[6] Conductivity (σ_x, σ_y, and σ_z, see notation section) is thus determined along three orthogonal axes in the core reference frame: z is vertical and x and y lie in the horizontal plane. The orientation of x and y axis relative to north is determined from magnetic remanence. Shipboard cryomagnetometer measurements after partial demagnetization in a 30 mT alternating field were obtained every 5 cm on the cores [*Moore et al.*, 2001]. These data are dense enough to allow reorientation of a majority of the measurements.

[7] All measurements were done at ambient conditions. The temperature in the laboratory was recorded during each sample measurement and varied between 24 and 29°C. A moderate pressure of about 1 bar was applied on the samples along the direction of measurement with a 10-pound weight. This applied pressure increased measurement reproducibility, and generally result in a small (less than 5%) increase of conductivity compared to measurements made without any applied pressure. Samples with apparent fissility displayed more sensitivity to pressure applied along the vertical axis, as cracks tend to open and fill with air when no pressure is applied.

[8] The measurement method does not give the complete electrical conductivity tensor, but only the diagonal terms in three directions. From these values, the horizontal anisotropy (a_H) or apparent anisotropy in the horizontal plane is defined as

$$a_H = 2(\sigma_x - \sigma_y)/(\sigma_x + \sigma_y), \tag{1}$$

and the vertical anisotropy (a_V) or average anisotropy over vertical planes as

$$a_V = 2\left(\frac{\sigma_x + \sigma_y}{2} - \sigma_z\right) \Big/ \left(\frac{\sigma_x + \sigma_y}{2} + \sigma_z\right). \tag{2}$$

Thus defined, the vertical anisotropy is invariant to rotation along the vertical axis, but this is not the case for the horizontal anisotropy. The anisotropy ratio (a) is defined the ratio of horizontal to vertical anisotropy:

$$a = a_H/a_V. \tag{3}$$

The normalized x axis conductivity (s_x) is defined as

$$s_x = 2\sigma_x/(\sigma_x + \sigma_y). \tag{4}$$

2.2. Results

[9] All measurements obtained on cube samples at Sites 1173 and 1174 are shown in Figure 2 along with porosity data and observations of bedding dip. In order to account for temperature variations in the lab, conductivity data are plotted as apparent formation factor, which is the ratio of seawater conductivity to sample conductivity at the same temperature ($F_a = \sigma_{seawater}/\sigma$). It is apparent both for Sites 1173 and 1174 that the vertical anisotropy follows the compaction trends. This is best illustrated in the Lower Shikoku Basis Facies, which is composed of fairly homogeneous hemipelagic sediments. If apparent formation factor is plotted against porosity, the vertical and horizontal components appear to follow different generalized Archie's laws, with different exponents (Figure 3). At Site 1174, the vertical conductivity of samples from the decollement and above plot on an intermediate trend suggesting that tectonic strain results in a lower vertical anisotropy than the normal compaction trend.

[10] Average horizontal anisotropy is zero, which is expected for random sample orientation. At Site 1173, horizontal anisotropy is generally low and may reflect the natural dispersion of the measurements (Figure 2). At Site 1174 the scatter of horizontal anisotropy is higher in the section above the decollement. In order to identify a component of anisotropy in the horizontal plane, the normalized x axis conductivity and the anisotropy ratio are plotted as a function of orientation for all reoriented samples from above the decollement level, including those located above the protothrust zone (Figure 4a). A small but significant anisotropy is found, corresponding in average to a 6.6% horizontal anisotropy or to an anisotropy ratio of 28%, determined from a least square fit of all reoriented data. The direction of maximum conductivity is N52°. No significant anisotropy is found below the decollement but a few anomalous high conductivities measured between N0° and

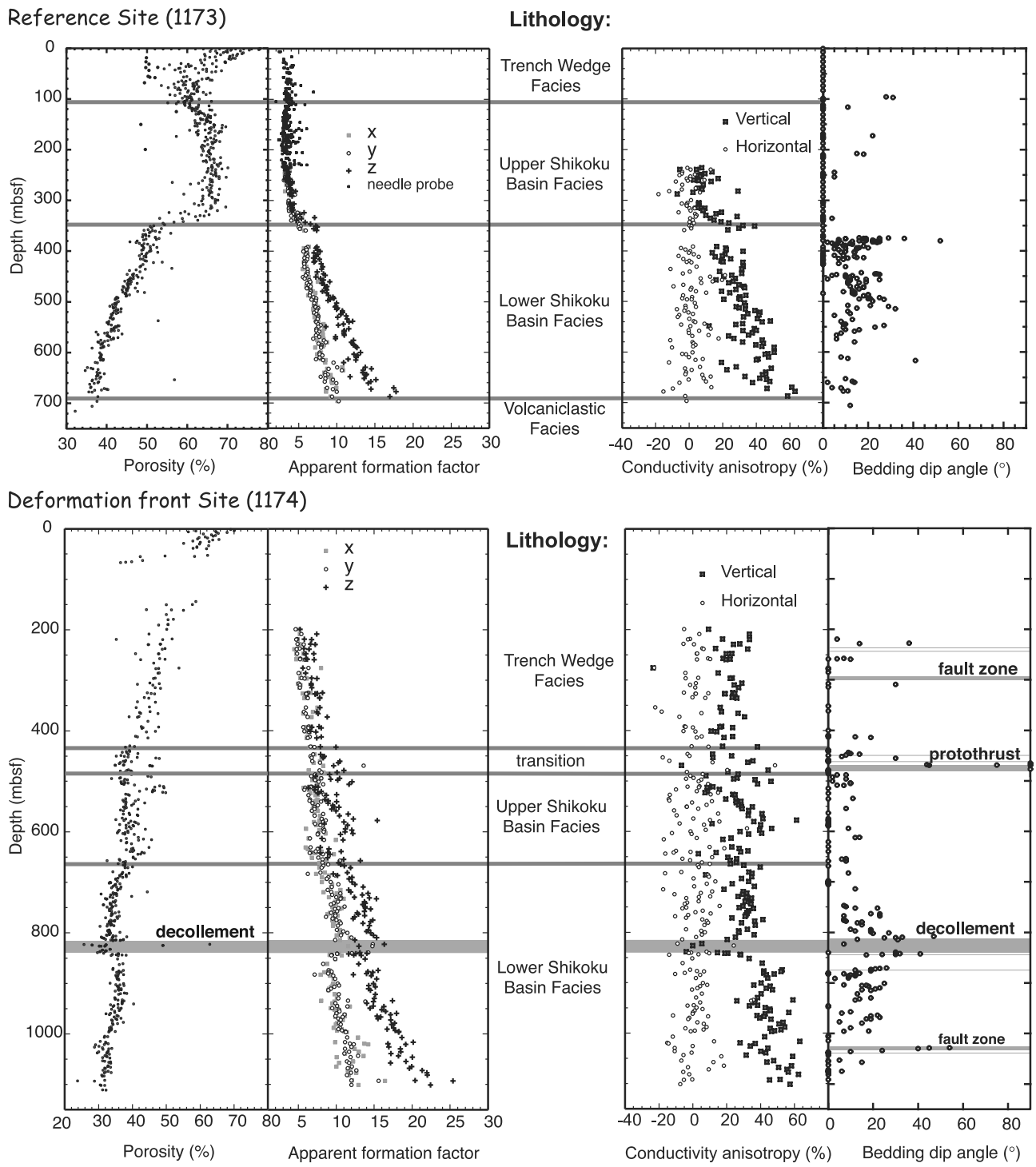

Figure 2. Measurements of apparent formation factor in all three directions (x, y, z) and of electrical conductivity horizontal and vertical anisotropy (see definitions in text) plotted next to porosity and bedding dip for Site 1173 (reference site) and Site 1174 (deformation front site). Needle probe measurements (using a four electrode array) were done on soft sediment cores from Site 1173 and did not measure significant anisotropy.

N20° may reflect discrete structures in these samples (Figure 4b).

2.3. Interpretation

[11] Interpretation of anisotropic physical properties in term of strain is based on the concept of an underlying relationship between fabric and anisotropy [*Owens and Bamford*, 1976]. Application of March's theory requires that the anisotropy signal is due to the reorientation of elongated or flat objects during nonisotropic strain. Clay particles and pores in clay matrix supported sediments, such as Nankai hemipelagites, are such objects. It is thus impor-

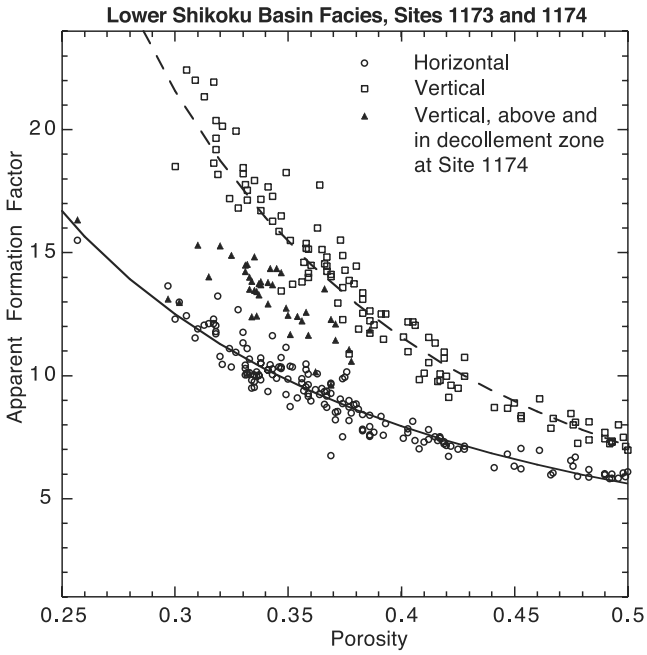

Figure 3. Apparent formation factors ($F_a = \sigma_{seawater}/\sigma$) versus porosity for Lower Shikoku Basin Facies at both sites. Best fitting Archie's law determined from reference site (1173) is $F_a = 1.87\phi^{-1.58}$ for the horizontal component and $F_a = 1.58\phi^{-2.17}$ for the vertical component. Measurements at Site 1174 (deformation front) below the decollement level follow the same trends. In the decollement zone and above, the average horizontal component follows the same trend, but the vertical one does not. We interpret this as a consequence of strain.

tant to test whether the measured anisotropy truly reflects the microstructure of the sample or is the consequence of larger scale cracking during unloading. Indeed, the observation that fissility affects the measurements suggests that cracking may contribute to the anisotropy signal. However, the most fissile samples are from the lower trench wedge at Site 1174 and they appear to have only moderate vertical anisotropy, of 10–30%. Samples from the lower part of the Shikoku Basin facies had no apparent fissility but have stronger anisotropy.

[12] Further evidence arises from measurements of surface conductivity. Surface conductivity in clay rich sediments occurs primarily along the surfaces or the edges of the clay particles. The anisotropy of surface conductivity should thus depend primarily on the anisotropy of the clay particle distribution. Because the relative contribution of surface conductivity to total sample conductivity decreases with salinity [*Clavier et al.*, 1977; *Revil et al.*, 1998], measurements performed with a high salinity pore fluid are insensitive to surface conductivity effects. The anisotropy of electrical conductivity measured at high salinity should thus depend on the anisotropy of the pore distribution. For the Nankai hemipelagic sediments, fluid conductivity is in the 4–5 S/m range at room temperature, pore conductivity is dominant, but the surface conductivity term is not negligible [*Bourlange et al.*, 2003]. Sodium surface conductivity was determined on a limited number of samples by exchanging the pore fluid with NaCl solutions of conductivity 10, 20, 6 and, 3 S/m. Samples were left to equilibrate about 2 months in each solution and the vertical anisotropy measured after equilibration is plotted against fluid conductivity in Figure 5. The plotted curves correspond to the linear high salinity asymptotes determined for each sample for the vertical direction ($\sigma_V = \sigma_z$) and for the average of horizontal directions ($\sigma_H = (\sigma_x + \sigma_y)/2$):

$$\sigma = \sigma_{fluid}/F + \sigma_{surface}. \quad (5)$$

[13] The anisotropy of surface conductivity is the value extrapolated on these curves at the limit of zero fluid conductivity, whereas the limit at infinite conductivity gives the anisotropy of pore fluid conductivity. Anisotropy changes little with pore fluid conductivity and the anisotropy of surface and pore fluid conductivity are of the same order. This suggests they both have the same origin. Furthermore, anisotropy tends to decrease with fluid conductivity in samples having a vertical anisotropy of more than 40%. If, hypothetically, the anisotropy signal were due to preferred unloading crack orientation, anisotropy should vanish when the conductivity of the pore fluid equals that of the clay matrix. As this condition may only be met near the zero salinity limit, anisotropy from unloading cracks should always increase with salinity in the range of measurements. As this is not the case, it is likely that unloading cracks only have a minor influence on anisotropy. Measurements also suggest that the distribution of orientation of clay particles and pores are similar. Anisotropy of electrical conductivity may thus be used to infer strain.

[14] Another problem arises from incomplete determination of tensor geometry. Because the electrical conductivity measurements were only performed along three directions, the complete anisotropy tensor cannot be determined unless the directions of the principal axes are assumed or independently known. The horizontal plane anisotropy measured above the decollement may either correspond to a tensor coaxial to the core axes or, hypothetically, to a noncoaxial case. However, it can at least be shown that the horizontal plane anisotropy measured between 485 and 745 mbsf is not just the consequence of strata dip. Tensor algebraic properties imply that the horizontal plane anisotropy and the anisotropy ratio are always sinusoidal functions of azimuth. Many samples have a high anisotropy ratio and the best fitting sinusoidal corresponds to an anisotropy ratio of 36% along a N58 azimuth (Figure 6). Assuming that the compacted sediment is originally transversely anisotropic with a vertical axis of symmetry, the anisotropy ratio is a function of the dip angle and is computed by applying a rotation to the conductivity tensor. A 36% anisotropy ratio would require a dip of about 30°. However, no dip larger than 15° has been measured in the interval between 485 and 745 mbsf. The anisotropy ratio predicted for a 15° dip is always less than 10% and is too low to explain observations (Figure 6). More likely, the anisotropy tensor has lost its axial symmetry during strain and, like the AMS tensor [*Owens*, 1993; *Hisamitsu et al.*, 2001], is nearly coaxial to the core axis. However,

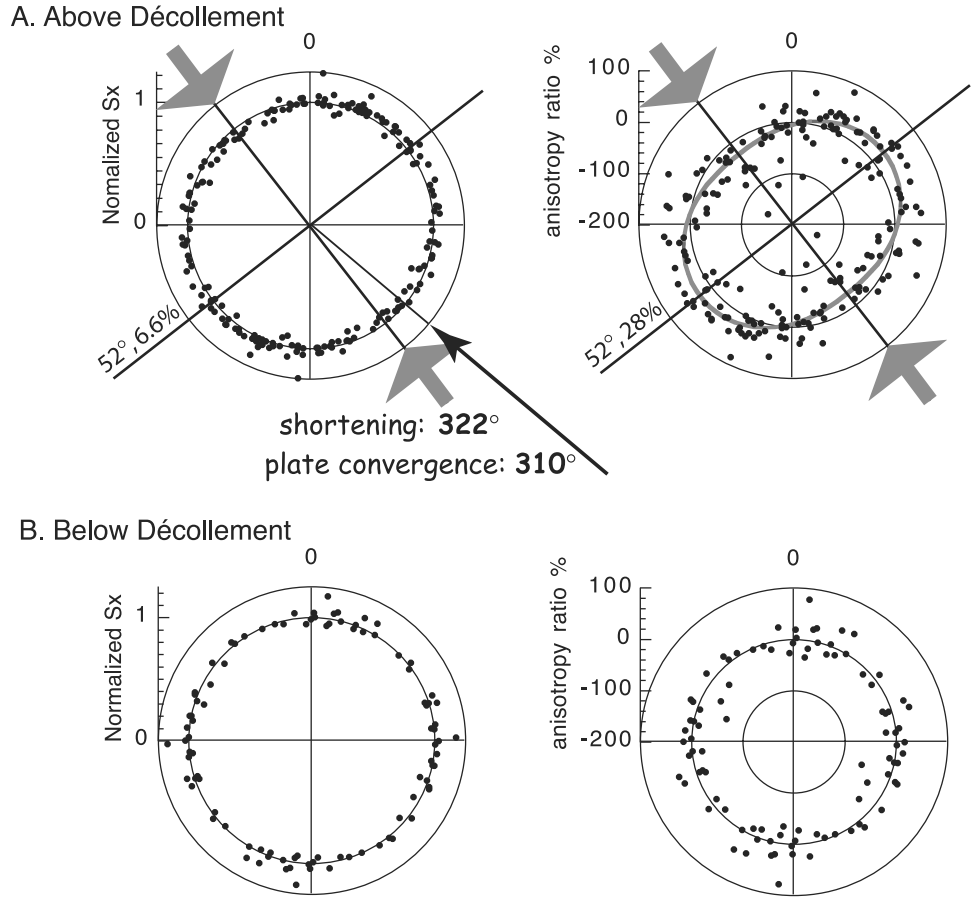

Figure 4. Polar plots of normalized conductivity and anisotropy ratio as a function of azimuth at the deformation front site (Site 1174). (a) Above the decollement. (b) Below the decollement. Data above the decollement display a maximum conductivity along a N52° direction, which is parallel to the deformation front and indicates ductile shortening along a N322° axis. Plate convergence is N310°.

one cannot exclude that the anisotropy signal in the zone from about 750 mbsf to the base of the decollement at 840 mbsf may also be affected by bedding dips.

3. Strain Computations

3.1. Assumptions and Definitions in March's Theory

[15] Relationships between strain and fabric in clay (or more generally phyllosilicates) can be obtained on the assumption that particles passively follow deformation, which is the fundamental assumption in March's theory (1932). This assumption is not generally valid because of electrostatic interaction between clay particles and recrystallization during diagenesis and metamorphism. It is also shown experimentally that large isotropic strains can destroy original anisotropy [*Kuganenthira et al.*, 1996], whereas it should have no effect according to March's theory. However, March's approach is considered as a good first approximation of strain even when there is extensive silicate recrystallization [*Evans et al.*, 1989]. Large isotropic strains are not expected at the Nankai sites except, perhaps, within the decollement zone.

[16] The orientation of a clay particle or of a flat pore is defined by the normal **n** to the particle or pore plane. When the material is subject to strain **S**, the assumption of passive reorientation results in the following equation [*Owens*, 1973]:

$$\mathbf{n}_{after} = \frac{{}^{t}\mathbf{S}^{-1} \cdot \mathbf{n}_{before}}{\| {}^{t}\mathbf{S}^{-1} \cdot \mathbf{n}_{before} \|}. \tag{6}$$

Note that **S** is a finite strain tensor and thus is I (not 0) in the absence of deformation. With this formula and for coaxial pure shear, the orientation of particles is not sensitive to the strain path but only to the finite strain between initial and final states.

[17] Two cases of strain are considered. Compaction strain is pure shear with vertical shortening and no strain on the horizontal axis. The strain tensor is a function of initial and final porosity:

$$\mathbf{S} = \begin{bmatrix} 1 & 0 & 0 \\ 0 & 1 & 0 \\ 0 & 0 & \dfrac{1-\phi_0}{1-\phi} \end{bmatrix}. \tag{7}$$

[18] Tectonic strain in the wedge may be approximated as horizontal pure shear, assuming all simple shear occurs within the decollement zone. Analysis of shear bands and slickenlined faults suggests that, in fact, the main principal

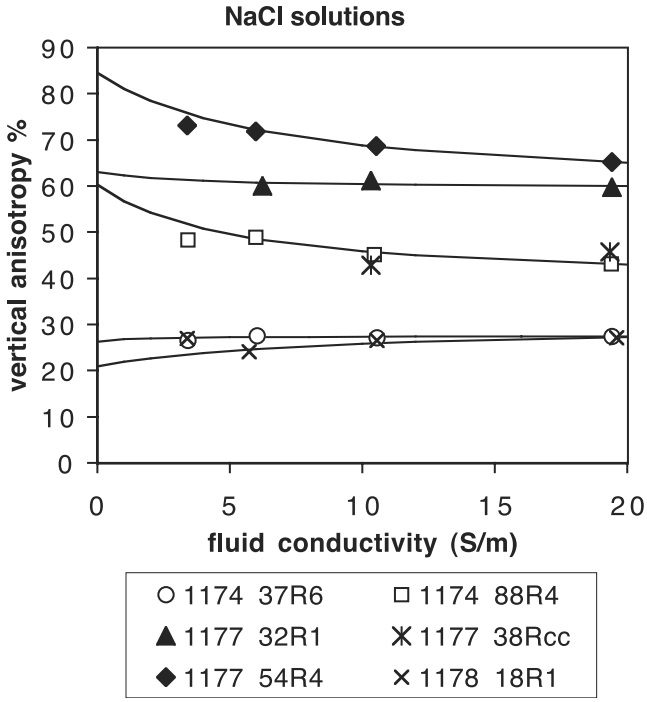

Figure 5. Vertical anisotropy as a function of conductivity of NaCl exchange solution. Fitting curves correspond to the high salinity asymptotes (see text).

stress axis dips slightly (up to 10°) during the phase of strain localization [*Moore et al.*, 2001]. The same may have been true during ductile distributed strain but this cannot be assessed with the electrical conductivity data because a small dip of the principal strain axis will not change results. In the horizontal pure shear model, the amount of horizontal shortening should be the same from the top of the column to the decollement. The strain tensor depends only on horizontal shortening and initial and final porosity:

$$\mathbf{S} = \begin{bmatrix} \frac{X}{X_0} & 0 & 0 \\ 0 & 1 & 0 \\ 0 & 0 & \frac{X_0}{X}\frac{1-\phi_0}{1-\phi} \end{bmatrix}. \quad (8)$$

3.2. Conductivity Anisotropy and Fabric: Assumptions and Model

[19] In order to relate the conductivity anisotropy with the fabric, let us assume that the pores in the clay matrix are flat and may be treated as disks conducting fluid only in their plane. For such a system, different physical approaches based on the noninteracting crack theory [*Kachanov*, 1993] or on a mean field approximation [*David*, 1985; *Gueguen and Dienes*, 1989; *Sausse et al.*, 2001] have resulted in a linear relationship between the permeability tensor and a tensor, $\boldsymbol{\alpha}$, that is a function of the pore distribution. The same approach can be applied to other transport properties such as the electrical conductivity tensor:

$$\boldsymbol{\sigma} = \sigma_i \mathbf{I} + C[(\mathrm{tr}\ \boldsymbol{\alpha})\mathbf{I} - \boldsymbol{\alpha}], \quad (9)$$

where σ_i represents the background conductivity (assumed isotropic) and C is a function of the geometry of the pores (which may not be ideal flat disks) and of the connectivity of the network. For electrical conductivity, $\boldsymbol{\alpha}$ is the sum of the contributions of surface and fluid conductivity for each disk shaped pore:

$$\boldsymbol{\alpha} = (1/V) \sum_{i:pore} v_i(\sigma_f + \Sigma_s/w_i)\mathbf{n}_i \otimes \mathbf{n}_i, \quad (10)$$

where V is rock volume, Σ_s is surface conductance, σ_f is fluid conductivity, and v_i and w_i are the volume and aperture of individual pores.

[20] In the assumed case, the flat disks represent the entire porous network and the background conductivity should be zero. For simplicity, we also assume that the distribution of orientation and the distribution of pore size (and aperture) are independent. Pore volume and pore aperture are thus replaced in equation (10) by their average, and (9) and (10) combined:

$$\boldsymbol{\sigma} = C\phi\sigma_f(1 + \Sigma_s/w\sigma_f)\left[\mathbf{I} - \frac{1}{N}\sum_{i\ pore} \mathbf{n}_i \otimes \mathbf{n}_i\right], \quad (11)$$

where ϕ is the porosity, w is average pore aperture, and N is the number of pores. The data that we model are dimensionless parameters (vertical anisotropy, horizontal anisotropy, anisotropy ratio and normalized x axis conductivity) that can be computed simply from the normalized anisotropy tensor:

$$\mathbf{A} = \left[\mathbf{I} - \frac{1}{N}\sum_{i\ pore} \mathbf{n}_i \otimes \mathbf{n}_i\right]. \quad (12)$$

3.3. Computation Results

[21] The anisotropy tensor is computed from a random realization of the pore distribution. An initially isotropic

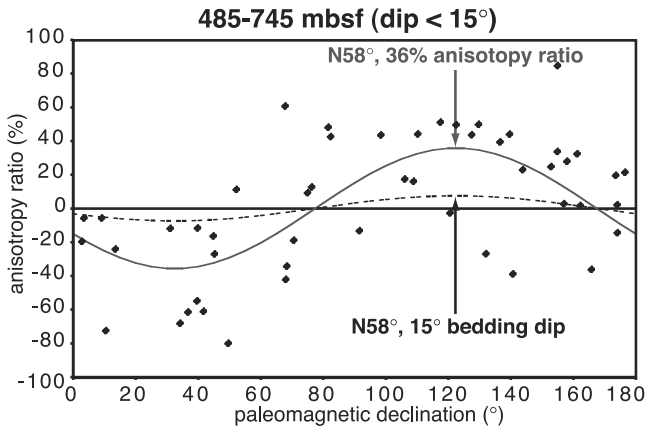

Figure 6. Comparison of the horizontal anisotropy ratio measured at Site 1174 between 485 and 745 mbsf and models. The maximum strata dip measured within this interval is 15°. Horizontal axis is magnetic declination and thus represents sample orientation. The solid curve is a best fit of the data assuming a fully anisotropic conductivity tensor (coaxial to the core axis). The dashed curve represents the anisotropy ratio that would result from tilting a transversely anisotropic medium by 15°.

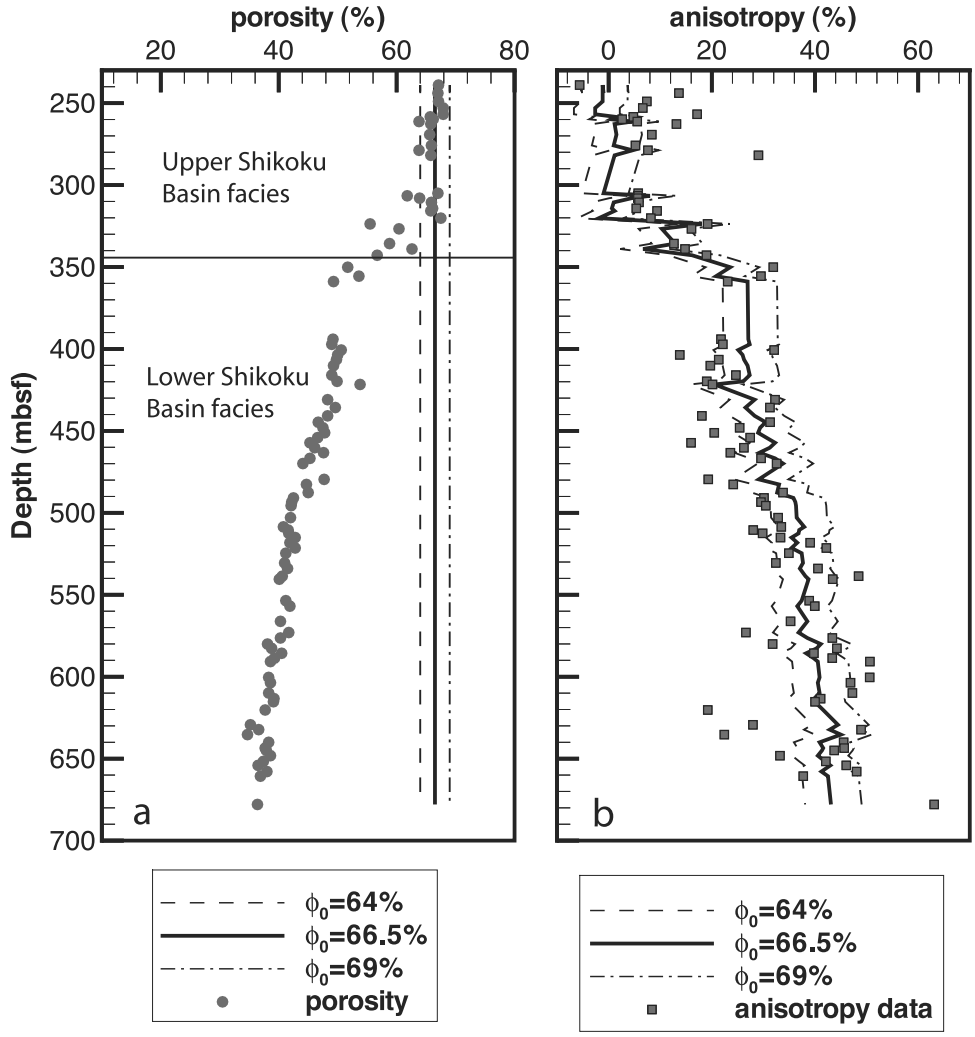

Figure 7. Predictions of compaction strain models at Site 1173 (reference site) and comparison with data. (a) Initial and final porosity. (b) Measured and computed vertical anisotropy.

population of 100,000 pores is defined by random determination of their normal vector. The strain operator is then applied to this distribution, following equation (6) and the anisotropy tensor is computed from equation (12).

[22] The method was first tested at Site 1173 (reference site), which presumably corresponds to a pure case of vertical compaction (equation (7)). The only adjustable parameter in this model is initial porosity ϕ_0. Computations are shown for three values of initial porosity (Figure 7). With an initial porosity of 69%, data from the Upper Shikoku Basin facies and the sharp change in porosity and anisotropy at its base are well fit. A lower initial porosity of 64% is required to fit data between 400 and 500 mbsf. The model with 66.5% initial porosity is the best fitting model if the entire depth range of data is considered. We conclude that this model is consistent with the behavior of the sediment during compaction.

[23] For Site 1174 (protothrust zone site) a vertical compaction model with an initial porosity of 67% approximates anisotropy data in the underthrust sequence (Figure 8). However, vertical anisotropy predicted with this compaction model is much too high in the section above the decollement. This observation and the horizontal anisotropy (see measurement section) were both used to constrain the amount of ductile strain using equation (8). This is also an important test of the method self-consistency. For moderate horizontal strains, the dependence of anisotropy on strain is close to linear and models with horizontal strain in the 10–15% range satisfy constraints on both horizontal and vertical anisotropy. Assuming 67% initial porosity, the best fitting model is with 12% shortening ($X/X_0 = 0.88$) (Figure 8). The computed horizontal anisotropy for this scenario is nearly constant but slightly decreases with depth from 6.8% at 200 mbsf to about 5.8% at 800 mbsf. The vertical anisotropy is within the range of data and follows, at least qualitatively, the variations in anisotropy associated with the high porosity intervals around 500 mbsf and 630 mbsf. The decollement zone itself appears as a zone of abnormally low anisotropy, which suggests additional strain not accounted for by the pure shear model.

3.4. Porosity Evolution

[24] Early occurrence of horizontal strain above the decollement suggests that the discontinuity in porosity observed across the decollement (4–5% at Site 1174, 5–6% at Site 808) is, at least in part, due to a discontinuity of

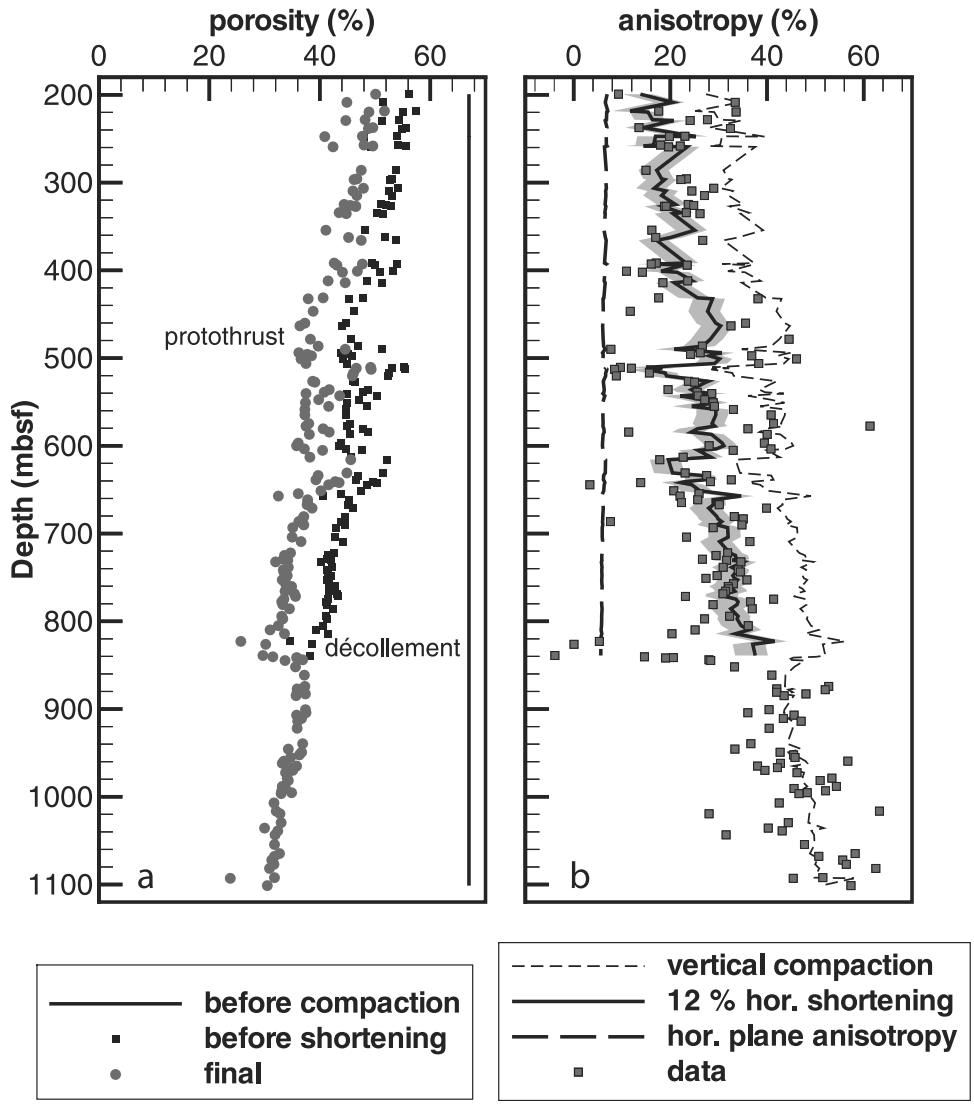

Figure 8. Predictions of strain models at Site 1174 (deformation front site) and comparison with data. (a) Porosity evolution. (b) Computed vertical anisotropy compared with data and the computed horizontal anisotropy. The gray area corresponds to the 10–15% range of horizontal strain, assuming 67% initial porosity. Horizontal anisotropy measurements are summarized on Figure 4.

the stress state [*Morgan and Karig*, 1995b]. In this hypothesis, ductile horizontal strain everywhere above the decollement should be associated with volume loss. As remarked in the assumptions and definitions section, the final state computed in the model does not depend on the strain path. However, it is possible to calculate the porosity at the beginning of horizontal shortening for different hypotheses. If horizontal shortening occurred under purely undrained conditions, the porosity before shortening is the final porosity. This would imply that the porosity jump existed even before shortening. If horizontal shortening is uniaxial (no associated thickening), then the porosity at the beginning of shortening is:

$$\phi_1 = 1 - \frac{X}{X_0}(1 - \phi). \tag{13}$$

If ductile horizontal strain is truly uniaxial, the thickening of the sedimentary layers observed on the seismic profiles requires additional distributed (or diffuse) strain. As noted by *Morgan and Karig* [1995a], this additional strain may be the consequence of slip on small-scale faults. The porosities (ϕ_1) computed from equation (13) are plotted on Figure 8 and lie in continuity with the trend defined by measurements from the underthrust sequence. This coincidence may be explained if the porosity profile at the time of decollement initiation reflected compaction of homogenous sediments in a smoothly varying pore pressure regime. It is not possible to demonstrate which scenario is correct form the data available. However, the presence of only a small (<2%) porosity jump at the reference site (Site 1173) suggests that the uniaxial horizontal strain scenario may be a better approximation. Average pore pressure ratio (λ) in the underthrust sequence at Site 1174 has been estimated to 0.66 (corresponding to excess pore pressure ratio $\lambda^* = 0.42$, see definitions in the notation section) based on the analysis of compaction curves [*Screaton et al.*, 2002]. This moderate

overpressuring is primarily due to sedimentary loading by rapid turbidite sedimentation in the trench [*Le Pichon et al.*, 1993; *Screaton et al.*, 2002] and may approximate the pore pressure regime in the formation on both sides of the decollement at the beginning of decollement initiation.

4. Discussion

[25] We showed that the evolution of electrical anisotropy with depth at the reference site follows the evolution of porosity. It also follows irregularities in the compaction curve. In the abyssal plain (Site 1173), a sharp porosity change at the lithological transition from Upper to Lower Shikoku Basin Facies corresponds to a sharp increase of anisotropy. This implies that the porosity change is associated with clay particle reorientation. At Site 1174, intervals of preserved high porosity are also found in the Upper Shikoku Basin Facies and correspond to zones of low anisotropy. Between these intervals, the sediment compacted and anisotropy increased. It is hypothesized that the evolution of porosity in the Upper Shikoku Basin Facies is controlled by silica diagenesis and that porosity loss is associated with a reorganization of the clay particles after the dissolution of grain contact cement [*Mikada et al.*, 2002; *Moore et al.*, 2001]. Observations on anisotropy of electrical conductivity agree well with this hypothesis.

[26] We estimate that about 12% subhorizontal ductile strain associated with porosity loss occurred at Site 1174 in the section above the decollement. Laboratory work on porous rocks shows that porosity exerts important control over the brittle-ductile transition [*Karig*, 1990; *Wong*, 1990]. Furthermore, triaxial tests on tuff samples from Nankai show that the amount of porosity reduction before failure is a function of effective stress [*Zhang et al.*, 1993]. We suggest that porosity reduction in the section above the decollement occurred prior to failure and could, in theory, be used to infer pore pressure conditions at failure. This, however, would require better laboratory constraints on the failure conditions in the hemipelagic lithologies.

[27] The results of the present study are also consistent with previous work that identified a change in strain axis orientation across the decollement at Nankai and Barbados wedge toes, using other methods such as AMS [*Housen*, 1997; *Owens*, 1993], X-ray goniometry [*Morgan and Karig*, 1993] and *P* wave anisotropy [*Brueckmann et al.*, 1993]. These results are consistent with new AMS results from Leg 190 [*Hisamitsu et al.*, 2001]. The underthrust sequence apparently continues to compact vertically whereas the entire sequence above the decollement is subject to horizontal strain. The present study also finds comparable quantitative estimates of ductile strain at Site 1174 (where deformation is at the protothrust stage) as previous work using X-ray goniometry at Site 808 (frontal thrust with 150 m throw) [*Morgan and Karig*, 1993]. This suggests that layer parallel shortening is 10–15% at both sites in spite of deformation processes being more advanced at Site 808 and strengthens the conclusion that ductile strain occurred prior to thrusting [*Morgan and Karig*, 1995a]. Furthermore, ductile horizontal shortening occurs both above and below the protothrust. It is thus shown that ductile strain occurs early in the process of strain localization in the section above the decollement and is not the consequence of thrust initiation (or propagation). However, distributed horizontal ductile strain (layer parallel shortening) should follow decollement initiation because it reflects strain decoupling.

[28] Comparison of results from anisotropy of electrical conductivity and X-ray goniometry is also interesting as a test of the methods. As noted in section 1, X-ray goniometry failed to give the correct vertical compaction strain [*Morgan and Karig*, 1993] and the anisotropy of electrical conductivity seems, with this respect, to give better results. One should note that the absence of a reference site in the earlier study may have been an obstacle to calibration but there are also fundamental differences. The X-ray goniometry is sensitive to clay particle orientation whereas the electrical method is mostly sensitive to pore orientation (at least for a high salinity pore fluid). We assumed that particles and pores have the same distribution of orientations and provided arguments in support of this hypothesis in the measurement interpretation section (section 2.3). We thus do not consider a discrepancy between particle and pore orientation distributions as the most likely explanation. The spatial resolution of methods is also different as the electrical method is sensitive to average pore orientation whereas X-ray goniometry may be affected by changes in crystalline network orientation at a scale smaller than particle size. Consequently, it is possible that the effect of small-scale crystalline disorder on the X-ray goniometry data partly masks the compaction signal. The X-ray goniometry method still appears sensitive to loss of axial symmetry during horizontal strain.

[29] The N052° direction of maximum conductivity in the section above the decollement implies shortening along a N322° direction, nearly perpendicular to the local strike of the deformation front and consistent with the anisotropy of magnetic susceptibility results [*Hisamitsu et al.*, 2001]. This direction is at a slight angle (12°) from the N310° direction of convergence [*Mazzotti et al.*, 2000; *Seno et al.*, 1993]. The direction of the principal stress axis inferred from slickenlined faults [*Lallemant et al.*, 1993] and deformation bands [*Ujiie et al.*, 2003] is closer to the direction of plate convergence. This suggests that some shear partitioning may be occurring even during strain localization. If ductile shortening is strictly normal to the trough axis, all of the small subduction obliquity must be taken up on faults.

[30] Layer parallel shortening at Site 1174 implies slip on the decollement seaward of the frontal thrust. The decollement reflector has strong amplitude below the trench wedge up to 5 km seaward of Site 1174. Deformation of the reflectors at the base of the trench wedge is observed on the seismic section up to the deformation front, 1.5 km seaward of Site 1174 (Figure 1). These may be considered as upper and lower bounds for the onset of sliding along the decollement. Assuming 10% horizontal shortening over 5 km, slip on the decollement due to ductile shortening alone may be as high as 500 m at Site 1174. Assuming shortening increases linearly from 0% to 10% over 1.5 km, a lower bound of 75 m for slip as Site 1174 is obtained. However, total slip is certainly larger due to thickening by small-scale deformation bands and faults. The decollement thus appears as the very first shear localization structure in

the system and is already a mature fault zone when imbricate thrusting is initiated.

5. Conclusions

[31] The anisotropy of electrical conductivity in clay rich sediment reflects the evolution of clay microfabric and can be used to quantify strain. At the toe of Nankai accretionary wedge, we estimate that 10–15% layer parallel shortening occurred before brittle failure in the entire section above the decollement.

[32] 1. In the abyssal plain (Site 1173), a sharp porosity change at the lithological transition from Upper to Lower Shikoku Basin Facies corresponds to a sharp increase of anisotropy. This very strong compaction gradient is thought to be a consequence of silica diagenesis.

[33] 2. Timing of deformation is as follows: (1) decollement initiation below the trench, (2) ductile layer parallel shortening in the section above the decollement, (3) strain localization in the section above the decollement, and (4) slip on imbricate thrusts. There may be some overlap between these phases. However, most of the ductile strain occurs after decoupled stress conditions are established at the decollement level and the decollement slips at least 150–500 m before significant slip occurs on the imbricate thrusts.

[34] 3. Layer parallel shortening is associated with porosity loss and can account for the change of porosity observed across the decollement. This also implies moderate pore overpressure in the formation above the decollement zone.

[35] 4. Fully understanding the process of decollement initiation would probably require drilling seaward of Site 1174, at a location where the decollement already acquired some reflectivity but where no deformation is apparent in the basin section.

Notation

σ	electrical conductivity.
σ_x	electrical conductivity along axis x (= σ_{xx} tensor term).
σ_H	average conductivity in horizontal plane (= $(\sigma_x+\sigma_y)/2$).
σ_V	conductivity along vertical axis (= σ_z).
a_H	horizontal anisotropy.
a_V	vertical anisotropy.
a	anisotropy ratio (= a_H/a_V).
s_x	normalized electrical conductivity along x axis (= σ_x/σ_H).
F_a	apparent formation factor (= $\sigma_{seawater}/\sigma$).
F	formation factor.
$\sigma_{surface}$	contribution of mineral surfaces to bulk conductivity.
$\mathbf{n}$	unit vector normal to particle or pore.
$\mathbf{S}$	strain tensor.
ϕ	porosity.
ϕ_0	initial porosity at deposition.
ϕ_1	porosity at the beginning of shortening.
X/X_0	horizontal strain.
σ_i	background conductivity (isotropic).
C	dimensionless conductivity factor.
$\mathbf{I}$	identity tensor.
$\boldsymbol{\alpha}$	pore distribution anisotropy tensor.
$\boldsymbol{\sigma}$	electrical conductivity tensor.
V	rock volume.
v_i	volume of pore i.
w_i	aperture of pore i.
σ_f	pore fluid conductivity (= σ_{fluid}).
Σ_s	surface conductance.
N	number of pores in volume V.
w	average aperture.
$\mathbf{A}$	normalized anisotropy tensor.
P_{fluid}	fluid pressure.
P_{hydro}	fluid hydrostatic pressure.
$P_{seafloor}$	pressure at the seafloor (hydrostatic).
P_{litho}	lithostatic pressure.
λ	pore pressure ratio $(P_{fluid} - P_{seafloor})/(P_{litho} - P_{seafloor})$.
λ^*	excess pore pressure ratio $(P_{fluid} - P_{hydro})/(P_{litho} - P_{hydro})$.

[36] **Acknowledgments.** We thank the leg 190 ODP crew for supporting an unrequired experiment and particularly Pieter Pretorius, who maintained the electrical resistivity device. We thank Maria Zamora at IPG Paris for advice and help with the determination of surface conductivities and Yves Gueguen (ENS Paris for theoretical discussions). We thank reviewers Julia Morgan, Peter Flemings, and Associate Editor Phil Wannamaker for their careful reading of the manuscript and their constructive comments. This work was supported by INSU "ad hoc ocean" fund.

References

Allmendinger, R. W., Inversed forward numerical modelling of trishear fault propagation fold, *Tectonics*, *17*, 640–656, 1998.

Averbuch, O., D. Frizon de Lamotte, and C. Kissel, Magnetic fabric as a structural indicator of the deformation path within a fold-thrust structure: A test case from the Corbière (NE Pyrenées France), *J. Struct. Geol.*, *14*, 461–474, 1992.

Beaumont, C., and G. Quinlan, A geodynamic framewok for interpreting crustal-scale seismic-reflectivity patterns in compressional orogens, *Geophys. J. Int.*, *116*, 754–783, 1994.

Besuelle, P., Compacting and dilating shear bands in porous rocks; theoretical and experimental conditions, *J. Geophys. Res.*, *106*, 13,435–13,442, 2001.

Bourlange, S., P. Henry, J. C. Moore, H. Mikada, and A. Klaus, Fracture porosity in the decollement zone of Nankai accretionary wedge using Logging While Drilling resistivity data, *Earth Planet. Sci. Lett.*, *209*, 103–112, 2003.

Brueckmann, W., K. Moran, and E. Taylor, Accoustic anisotropy and microfabric development in accreted sediment from the Nankai Trough, *Proc. Ocean Drill. Program Sci. Results*, *131*, 221–233, 1993.

Clavier, C., G. Coates, and J. Dumanoir, The theoretical and experimental bases for the dual-water model for the interpretation of shaly sands, paper presented at SPE 52nd Annual Fall Technical Conference, Soc. of Pet. Eng., Denver, Colo., 1977.

David, C., Modèle d'évolution de la permeabilité d'une roche, DEA thesis, Univ. Louis Pasteur, Strasbourg, France, 1985.

Doin, M. P., and P. Henry, Subduction initiation and continental crust recycling: The roles of rheology and eclogitization, *Tectonophysics*, *342*, 163–191, 2001.

Evans, K. F., G. Oertel, and T. Engelder, Apalachian stress study: 2. Analysis of Devonian shale core: Some implications for the nature of contemporary stress variations and Alleghanian deformation in Devonian rocks, *J. Geophys. Res.*, *94*, 7155–7170, 1989.

Frizon de Lamotte, D., Early record of tectonic magnetic fabric during inversion of a sedimentary basin. Short review and examples from the Corbières transfer zone (France), *Bull. Soc. Geol. Fr.*, *173*, 461–469, 2002.

Gueguen, Y., and J. Dienes, Transport properties of rocks from statistics and percolation, *Math. Geol.*, *21*, 1–13, 1989.

Henry, P., Relationship between porosity, electrical conductivity, and cation exchange capacity in Barbados wedge sediments, *Proc. Ocean Drill. Program Sci. Results*, *156*, 137–149, 1997.

Hisamitsu, T., K. Ujiie, and A. Taira, Magnetic fabric analysis of proto-decollement zone at the toe of the Nankai accretionary prism, *Eos Trans. AGU*, *82*(47), Fall Meet. Suppl., Abstract T41A-0857, 2001.

Housen, B. A., Magnetic anisotropy of Barbados prism sediments, *Proc. Ocean Drill. Program Sci. Results*, *156*, 97–105, 1997.

Kachanov, M., Elastic solids with many cracks and related problems, *Adv. Appl. Mech.*, *30*, 259–445, 1993.

Karig, D.E., Experimental and observational constrains on the mechanical behavior in the toes of accretionary prisms, in *Deformation Mechanisms, Rheology and Tectonics*, edited by R. J. Knipe and E. H. Rutter, *Geol. Soc. Spec. Publ.*, *54*, 383–398, 1990.

Karig, D. E., and J. K. Morgan, Tectonic deformation; stress paths and strain histories, in *The Geological Deformation of Sediments*, edited by A. Maltman, pp. 167–204, Chapman and Hall, New York, 1994.

Kuganenthira, N., D. Zhao, and A. Anandarajah, Measurement of fabric anisotropy in triaxial shearing, *Géotechnique*, *46*, 657–670, 1996.

Lallemant, S. J., T. Byrne, A. Maltman, D. Karig, and P. Henry, Stress tensors at the toe of the Nankai accretionry prism: An application of inverse methods to slickenlined faults, *Proc. Ocean Drill. Program Sci. Results*, *131*, 103–122, 1993.

Le Pichon, X., P. Henry, and S. Lallemant, Accretion and erosion in subduction zones: The role of fluids, *Annu. Rev. Earth Sci.*, *21*, 307–331, 1993.

Mazzotti, S., X. Le Pichon, P. Henry, and S.-I. Miyazaki, Full interseismic locking of the Nankai and Japan-west Kurile subduction zones: An analysis of uniform elastic strain accumulation in Japan constrained by permanent GPS, *J. Geophys. Res.*, *105*, 13,159–13,177, 2000.

Mikada, H., J. C. Moore, K. Becker, and A. Klaus, *Proceedings of the Ocean Drilling Program*, *Initial Reports*, vol. 196, Ocean Drill. Program, College Station, Tex., 2002.

Moore, G. F., A. Taira, and A. Klaus, *Proceedings of the Ocean Drilling Program, Initial Reports,* vol. 190, Ocean Drill. Program, College Station, Tex., 2001.

Morgan, J. K., and D. E. Karig, Ductile strains in clay-rich sediments from hole 808C: Preliminary results using X-ray pole figure goniometry, *Proc. Ocean Drill. Program Sci. Results*, *131*, 141–155, 1993.

Morgan, J. K., and D. E. Karig, Kinematics and a balanced cross-section across the toe of the eastern Nankai accretionary prism, *J. Struct. Geol.*, *17*, 31–45, 1995a.

Morgan, J. K., and D. E. Karig, Decollement processes at the Nankai accretionary margin, southeast Japan: Propagation, deformation, and dewatering, *J. Geophys. Res.*, *100*, 15,221–15,231, 1995b.

Owens, W. H., Strain modification of angular density distribution, *Tectonophysics*, *16*, 249–261, 1973.

Owens, W. H., Magnetic fabric studies of samples from Hole 808C, Nankai Trough, *Proc. Ocean Drill. Program Sci. Results*, *131*, 301–310, 1993.

Owens, W. H., and D. Bamford, Magnetic, seismic and other anisotropic properties of rock fabrics, *Philos. Trans. R. Soc. London, Ser. A*, *283*, 55–68, 1976.

Revil, A., L. M. Cathles, S. Losh, and J. A. Nunn, Electrical conductivity in shaly sands with geophysical applications, *J. Geophys. Res.*, *103*, 23,925–23,936, 1998.

Rochette, P., M. Jackson, and A. Aubourg, Rock magnetism and the interpretation of anisotropy of magnetic susceptibility, *Rev. Geophys.*, *30*, 209–226, 1992.

Rudnicki, J. W., and J. R. Rice, Conditions for the localisation of the deformation in pressure sensitive dilatant materials, *J Mech. Phys. Solids*, *23*, 371–394, 1975.

Sagnotti, L., F. Speranza, A. Winkler, M. Mattei, and R. Funiciello, Magnetic fabric of clay sediments from the external northern Apennines (Italy), *Physics Earth Planet. Inter.*, *105*, 73–93, 1998.

Saint-Bezar, B., R. L. Hebert, C. Aubourg, P. Robion, R. Swennen, and D. Frizon de Lamotte, Magnetic fabric and petrographic investigation of hematite-bearing sandstones within ramp-related folds: Examples from the south Atlas Front (Morocco), *J. Struct. Geol.*, *24*, 1507–1520, 2001.

Sausse, J., E. Jacquot, B. Fritz, J. Leroy, and M. Lespinasse, Evolution of crack permeability during fluid-rock interaction. Example of the Brézouard granite (Vosges, france), *Tectonophysics*, *336*, 199–214, 2001.

Screaton, E. J., et al., Porosity loss within the underthrust sediments of the Nankai accretionary complex: Implications for overpressures, *Geology*, *30*(1), 19–22, 2002.

Seno, T., S. Stein, and A. E. Gripp, A model for the motion of the Philippine Sea Plate consistent with NUVEL 1 and geological data, *J. Geophys. Res.*, *98*, 17,941–17,948, 1993.

Suppe, J., *Principles of Structural Geology*, 537 pp., Prentice-Hall, Old Tappan, N. J., 1985.

Ujiie, K., A. J. Maltman, M. Sanchez-Gomez, T. Hisamitsu, and T. Nakano, Nature, distribution, and origin of deformation bands at the toe of the active accretionary prism, *J. Struct. Geol.*, in press, 2003.

Wong, T.-F., Mechanical compaction and brittle-ductile transition in porous sandstones, in *Deformation Mechanisms, Rheology and Tectonics*, edited by R. J. Knipe and E. H. Rutter, *Geol. Soc. Spec. Publ.*, *54*, 111–122, 1990.

Zhang, J., D. M. Davis, and T.-F. Wong, Failure modes of tuff samples from Leg 131 in the Nankai accretionary wedge, *Proc. Ocean Drill. Program Sci. Results*, *131*, 275–281, 1993.

P. Henry, Departement de Geodynamique, College de France, Europole de l'Arbois, Batiment Laennec, hall D, etage 2, BP 80, F-13545 Aix en Provence, France. (henry@geologie.ens.fr)

S. Hunze, Geowissenschaftliche Gemeinschaftsaufgaben-GCA, Stilleweg 2, D-30631 Hannover, Germany. (s.hunze@gga-hannover.de)

L. Jouniaux, Laboratoire de Géologie, Ecole Normale Supérieure, CNRS UMR 8538, 24 rue Lhomond, F-75231 Paris Cedex 05, France.

D. M. Saffer, Department of Geology and Geophysics, P.O. Box 3006, University of Wyoming, Laramie, WY 82071-3006, USA. (dsaffer@uwyo.edu)

E. J. Screaton, Department of Geology, University of Florida, P.O. Box 112120, Gainesville, FL 32611, USA. (screaton@geology.ufl.edu)